

Peculiarities in pseudo-transitions of a mixed spin-(1/2, 1) Ising-Heisenberg double-tetrahedral chain in an external magnetic field

Onofre Rojas,¹ Jozef Strečka,² Oleg Derzhko,³ and S. M. de Souza¹

¹*Departamento de Física, Universidade Federal de Lavras, CP 3037, 37200-000, Lavras-MG, Brazil*

²*Department of Theoretical Physics and Astrophysics, Faculty of Science, P. J. Šafárik University, Park Angelinum 9, 040 01 Košice, Slovakia*

³*Institute for Condensed Matter Physics, National Academy of Sciences of Ukraine, Svientsitskii Str. 1, 79011 L'viv, Ukraine*

Abstract

Recently, it has been rigorously verified that several one-dimensional (1D) spin models may exhibit a peculiar pseudo-transition accompanied with anomalous response of thermodynamic quantities in a close vicinity of pseudo-critical temperature. In the present work we will introduce and exactly solve a mixed spin-(1/2,1) Ising-Heisenberg double-tetrahedral chain in an external magnetic field as another particular example of 1D lattice-statistical model with short-range interactions that displays a pseudo-transition of this type. The investigated model exhibits at zero temperature three ferrimagnetic phases, three frustrated phases, and one saturated paramagnetic phase. The ground-state phase diagram involves five unusual interfaces (phase boundaries), at which the residual entropy per site equals to a larger entropy of one of two coexisting phases. Four such interfaces are between a non-degenerate ferrimagnetic phase and a macroscopically degenerate frustrated phase, while one interface is between two non-degenerate ferrimagnetic phases. Though thermal excitations typically destroy all fingerprints of zero-temperature phase transitions of 1D lattice-statistical models with short-range forces, the mixed spin-(1/2,1) Ising-Heisenberg double-tetrahedral chain is quite robust with respect to thermal excitations and it displays peculiar pseudo-transitions close to all five aforementioned interfaces.

PACS numbers: 05.70.Fh, 75.10.-b, 75.10.Jm, 75.10.Pq

Keywords: Residual entropy; Quasi-phases; Pseudo-transitions; Ising-Heisenberg

I. INTRODUCTION

There are a few paradigmatic examples of one-dimensional (1D) lattice-statistical models with short-range couplings, which exhibit a discontinuous (first-order) phase transition at finite temperature. Perhaps the most famous example is 1D KDP model of hydrogen-bonded ferroelectrics invented by Nagle [1], which displays a discontinuous phase transition between the ferroelectric and paraelectric phases due to assignment of an infinite energy to all ionized configurations. Another particular example of this type is the Kittel model [2] defined through a finite transfer matrix, which involves a constraint on zipper corresponding to an infinite potential being responsible for a non-analyticity of the free energy. Owing to a singular character of the potential, the Kittel model also exhibits a first-order phase transition. The next paradigmatic example is the 1D solid-on-solid model considered by Chui and Weeks [3], which is exactly solvable in spite of an infinite dimension of its transfer matrix. By imposing suitable pinning potential the 1D solid-on-solid model may also display a roughening phase transition of first order [3]. Furthermore, Dauxois and Peyrard [4] have examined another 1D lattice-statistical model with an infinite dimension of the transfer matrix, which exhibits a phase transition at finite temperature. Last but not least, Sarkanych *et al.* [5] proposed 1D Potts model with so-called invisible states and short-range couplings. It could be thus concluded that all five aforementioned 1D lattice-statistical models break the Perron-Frobenius theorem, because some off-diagonal transfer-matrix elements become null and the

free energy may consequently become non-analytic at a certain critical temperature.

Van Hove [6] proposed a theorem that proves absence of a phase transition in 1D lattice-statistical models with short-range couplings. Later, Cuesta and Sanchez [7] generalized the non-existence theorem for a phase transition at finite temperatures. Surely, this is not yet the most general non-existence theorem, because mixed-particle chains or more general external fields fall beyond the scope of this theorem.

The term "pseudo-transition" and "quasi-phase" was introduced by Timonin [8] in 2011 when studying the spin-ice model in a field. These terms refer to a sudden change in first derivatives and vigorous peaks in second derivatives of the free energy although these marked signatures are not in reality true discontinuities and divergences, respectively. Note furthermore that the pseudo-transitions do not violate the Perron-Frobenius theorem, because the free energy is always analytic. A common feature of the pseudo-transitions is that some off-diagonal transfer-matrix elements (Boltzmann factors) become very small (almost zero), since very high albeit finite energy is assigned to the corresponding states.

Obvious fingerprints of pseudo-transitions were recently found in several 1D spin or spin-electron models. For instance, the pseudo-transitions were detected in the spin-1/2 Ising-Heisenberg diamond chain [9, 10], two-leg ladder [11], as well as triangular tube [12]. Similarly, the emergence of pseudo-transitions was verified in the spin-1/2 Ising diamond chain [13] and the coupled spin-electron double-tetrahedral chain [14–16]. In general, the first derivatives of the free energy such as entropy, inter-

nal energy or magnetization show a steep change around pseudo-critical temperature. This feature is similar to the first-order phase transition, but all thermodynamic response functions are in fact continuous. Contrary to this, second derivatives of the free energy such as specific heat and magnetic susceptibility resemble typical behavior of a second-order phase transition at a finite temperature. Therefore, this peculiar pseudo-critical behavior drew attention to a more comprehensive study of this phenomenon aimed at elucidating all its essential features [17–19]. Recently, a further attention has been paid to uncover the mechanism triggering pseudo-transitions based on a rigorous analysis of the correlation function [10] and pseudo-critical exponents [20].

The goal of the present study is to investigate a mixed spin-(1/2,1) Ising-Heisenberg tetrahedral chain in an external magnetic field, which has a pretty rich ground-state phase diagram and exhibits a number of finite-temperature pseudo-transitions close to some inter-phase boundaries. There are some 3D compounds in which, when we consider one columnar stripe, we could observe a double tetrahedral chain structure. Such as cobalt oxide RBaCo_4O_7 , where R denotes a rare earth atom, which has a swedenborgite lattice structure[21]. Another compound with a similar structure could be the salt with 3D corrugated packing frustrated spin [22] of $\text{C}_{60}^{\bullet-}$ in $(\text{MDABCO}^+)(\text{C}_{60}^{\bullet-})$ [$\text{MDABCO}^+ = N$ -methyl diazabicyclooctanium cation and $\text{C}_{60}^{\bullet-}$ radical anions], a stripe of this salt can be viewed also as a double-tetrahedral chain.

This article is organized as follows. In Sec. II we consider and exactly solve the mixed spin-(1/2,1) Ising-Heisenberg tetrahedral chain in a magnetic field. Thermodynamics in a close vicinity of the pseudo-transition is examined in Sec. III, where an influence of the residual entropy upon basic thermodynamic quantities is investigated in detail. Finally, several concluding remarks are presented in Sec. IV.

II. MIXED SPIN-(1/2,1) ISING-HEISENBERG DOUBLE-TETRAHEDRAL CHAIN

The coupled spin-electron model on a double-tetrahedral chain [14–16], which involves localized Ising spins at nodal lattice sites and mobile electrons delocalized over triangular plaquettes, represents a prominent example of 1D lattice-statistical model mimicking a temperature-driven phase transition [14]. However, earlier investigations of the analogous spin-1/2 Heisenberg [23–25] and Ising-Heisenberg [26, 27] models on a double-tetrahedral chain did not verify anomalous thermodynamic response closely related to a pseudo-transition until the latter Ising-Heisenberg model was revisited and more thoroughly studied [18].

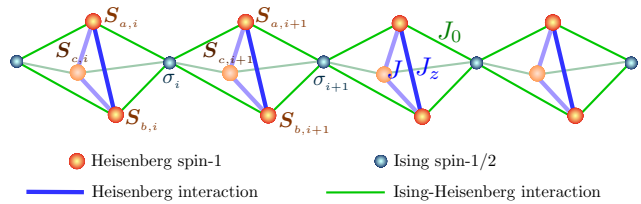


Figure 1: A schematic representation of the mixed spin-(1/2,1) Ising-Heisenberg double-tetrahedral chain. Small balls correspond to the Ising spins σ_i and large balls correspond to the Heisenberg spins $\mathbf{S}_{\gamma,i}$ ($\gamma = a, b, c$).

In the present work we will examine in particular the mixed spin-(1/2,1) Ising-Heisenberg double-tetrahedral chain, which is schematically depicted in Fig. 1 and defined through the following Hamiltonian

$$H = \sum_{i=1}^N H_i, \quad (1)$$

with

$$H_i = -[J(\mathbf{S}_{b,i}, \mathbf{S}_{c,i})_z + J(\mathbf{S}_{c,i}, \mathbf{S}_{a,i})_z + J(\mathbf{S}_{a,i}, \mathbf{S}_{b,i})_z] - (S_{a,i}^z + S_{b,i}^z + S_{c,i}^z)[h_z + J_0(\sigma_i + \sigma_{i+1})] - \frac{\hbar}{2}(\sigma_i + \sigma_{i+1}). \quad (2)$$

In above, $S_{\gamma,i}^\alpha$ ($\alpha = \{x, y, z\}$, $\gamma = \{a, b, c\}$) denote the spin-1 Heisenberg atoms, $\sigma_i = \pm \frac{1}{2}$ denotes the Ising spin, and $J(\mathbf{S}_{\gamma,i}, \mathbf{S}_{\delta,i})_z = JS_{\gamma,i}^x S_{\delta,i}^x + JS_{\gamma,i}^y S_{\delta,i}^y + J_z S_{\gamma,i}^z S_{\delta,i}^z$. The Hamiltonian (2) is written as a sum of cell Hamiltonians H_i , which correspond to spin clusters with the geometric shape of two face-sharing tetrahedra (i.e., trigonal bipyramid).

The overall Hilbert space of the mixed spin-(1/2,1) Ising-Heisenberg double-tetrahedral chain splits into several disjoint (orthogonal) subspaces, because the Hamiltonians H_i from different unit cells commute with each other. The Hilbert subspace corresponding to the spin-1 Heisenberg triangle from the i -th unit cell is given by the Hamiltonian matrix of dimension 27×27 and it can be further split into several smaller block-diagonal matrices depending on the z -component of the total spin: for $S_t^z = 0$ one has one 7×7 block matrix, for $|S_t^z| = 1$ two 6×6 matrices, for $|S_t^z| = 2$ two 3×3 matrices, and for $|S_t^z| = 3$ two 1×1 matrices. All eigenvalues and eigenvectors of spin-1 Heisenberg triangle Hamiltonian are listed in Table I. The first column stands for the eigenvalues of the S_t^z operator, while the counter k is used just to distinguish the states with same eigenvalues and the respective state degeneracy g_k in fourth column. With the help of eigenvalues and eigenvectors of the spin-1 Heisenberg triangle reported in Table I one can express the full energy spectrum per H_i unit cell of the mixed spin-(1/2,1) Ising-Heisenberg double-tetrahedral chain as follows

$$\varepsilon_k(\sigma_i, \sigma_{i+1}) = \varepsilon_k - \left(J_0 S_t^z + \frac{\hbar}{2} \right) (\sigma_i + \sigma_{i+1}). \quad (3)$$

Here, ϵ_k marks the respective eigenvalue of the spin-1 Heisenberg triangle listed in Table I.

Table I: Full spectrum of the spin-1 Heisenberg triangle specified according to the respective eigenvalue, state degeneracy, and eigenvector. The eigenstates are grouped according to the z -component of the total spin $S_t^z = S_a^z + S_b^z + S_c^z$. The first column stands for the eigenvalues of the S_t^z operator, and the second column is just to distinguish the eigenvector with the same S_t^z . The definition of mixing angles: $\cot(2\phi_1) = \frac{J_z - J}{2J}$, $\cot(2\phi_2) = \frac{J_z + 2J}{4J}$, and $\cot(2\phi_3) = \frac{J_z - 2J}{2\sqrt{6}J}$.

$ S_t^z\rangle$	k	Energy (ϵ_k)	g_k	State
0	0	$J + J_z$	2	$ 0,0\rangle = \left\{ \frac{1}{2} \left(\begin{pmatrix} 1 \\ 0 \\ -1 \end{pmatrix} - \begin{pmatrix} 0 \\ 1 \\ -1 \end{pmatrix} - \begin{pmatrix} 0 \\ -1 \\ 1 \end{pmatrix} + \begin{pmatrix} -1 \\ 0 \\ 1 \end{pmatrix} \right) \right.$ $\left. \frac{\sqrt{3}}{6} \left(2 \begin{pmatrix} 1 \\ 0 \\ -1 \end{pmatrix} - \begin{pmatrix} 1 \\ 0 \\ -1 \end{pmatrix} - \begin{pmatrix} 0 \\ 1 \\ -1 \end{pmatrix} - \begin{pmatrix} 0 \\ -1 \\ 1 \end{pmatrix} - \begin{pmatrix} -1 \\ 0 \\ 1 \end{pmatrix} + 2 \begin{pmatrix} -1 \\ 0 \\ 1 \end{pmatrix} \right) \right\}$
	1	$J\sqrt{6} \cot \phi_3$	1	$ 0,1\rangle = \frac{\sqrt{6}}{6} \cos \phi_3 \left(\begin{pmatrix} 1 \\ 0 \\ -1 \end{pmatrix} + \begin{pmatrix} 0 \\ 1 \\ -1 \end{pmatrix} + \begin{pmatrix} 0 \\ 1 \\ -1 \end{pmatrix} + \begin{pmatrix} 0 \\ 1 \\ -1 \end{pmatrix} + \begin{pmatrix} -1 \\ 0 \\ 1 \end{pmatrix} + \begin{pmatrix} -1 \\ 0 \\ 1 \end{pmatrix} \right) - \sin \phi_3 \begin{pmatrix} 0 \\ 0 \\ 0 \end{pmatrix}$
	2	$-J\sqrt{6} \tan \phi_3$	1	$ 0,2\rangle = \frac{\sqrt{6}}{6} \sin \phi_3 \left(\begin{pmatrix} 1 \\ 0 \\ -1 \end{pmatrix} + \begin{pmatrix} 1 \\ 0 \\ -1 \end{pmatrix} + \begin{pmatrix} 0 \\ 1 \\ -1 \end{pmatrix} + \begin{pmatrix} 0 \\ 1 \\ -1 \end{pmatrix} + \begin{pmatrix} -1 \\ 0 \\ 1 \end{pmatrix} + \begin{pmatrix} -1 \\ 0 \\ 1 \end{pmatrix} \right) + \cos \phi_3 \begin{pmatrix} 0 \\ 0 \\ 0 \end{pmatrix}$
	3	$-J + J_z$	2	$ 0,3\rangle = \left\{ \frac{1}{2} \left(- \begin{pmatrix} 1 \\ 0 \\ -1 \end{pmatrix} - \begin{pmatrix} 0 \\ 1 \\ -1 \end{pmatrix} + \begin{pmatrix} 0 \\ 1 \\ -1 \end{pmatrix} + \begin{pmatrix} -1 \\ 0 \\ 1 \end{pmatrix} \right) \right.$ $\left. \frac{\sqrt{3}}{6} \left(-2 \begin{pmatrix} 1 \\ 0 \\ -1 \end{pmatrix} - \begin{pmatrix} 1 \\ 0 \\ -1 \end{pmatrix} - \begin{pmatrix} 0 \\ 1 \\ -1 \end{pmatrix} + \begin{pmatrix} 0 \\ 1 \\ -1 \end{pmatrix} + \begin{pmatrix} -1 \\ 0 \\ 1 \end{pmatrix} + 2 \begin{pmatrix} -1 \\ 0 \\ 1 \end{pmatrix} \right) \right\}$
	4	$2J + J_z$	1	$ 0,4\rangle = \frac{\sqrt{6}}{6} \left(- \begin{pmatrix} 1 \\ 0 \\ -1 \end{pmatrix} + \begin{pmatrix} 1 \\ 0 \\ -1 \end{pmatrix} + \begin{pmatrix} 0 \\ 1 \\ -1 \end{pmatrix} - \begin{pmatrix} 0 \\ 1 \\ -1 \end{pmatrix} - \begin{pmatrix} -1 \\ 0 \\ 1 \end{pmatrix} + \begin{pmatrix} -1 \\ 0 \\ 1 \end{pmatrix} \right)$
1	5	$-2J(1 - \cot \phi_2) \pm h_z$	1	$ \pm 1,0\rangle = \frac{\sqrt{3}}{3} \left[\cos \phi_2 \left(\begin{pmatrix} \pm 1 \\ \pm 1 \\ \mp 1 \end{pmatrix} + \begin{pmatrix} \pm 1 \\ \mp 1 \\ \pm 1 \end{pmatrix} + \begin{pmatrix} \mp 1 \\ \pm 1 \\ \pm 1 \end{pmatrix} \right) - \sin \phi_2 \left(\begin{pmatrix} \pm 1 \\ 0 \\ 0 \end{pmatrix} + \begin{pmatrix} 0 \\ \pm 1 \\ 0 \end{pmatrix} + \begin{pmatrix} 0 \\ 0 \\ \pm 1 \end{pmatrix} \right) \right]$
	6			
	7	$-2J(1 + \tan \phi_2) \pm h_z$	1	$ \pm 1,1\rangle = \frac{\sqrt{3}}{3} \left[\sin \phi_2 \left(\begin{pmatrix} \pm 1 \\ \pm 1 \\ \mp 1 \end{pmatrix} + \begin{pmatrix} \pm 1 \\ \mp 1 \\ \pm 1 \end{pmatrix} + \begin{pmatrix} \mp 1 \\ \pm 1 \\ \pm 1 \end{pmatrix} \right) + \cos \phi_2 \left(\begin{pmatrix} \pm 1 \\ 0 \\ 0 \end{pmatrix} + \begin{pmatrix} 0 \\ \pm 1 \\ 0 \end{pmatrix} + \begin{pmatrix} 0 \\ 0 \\ \pm 1 \end{pmatrix} \right) \right]$
	8			
	9	$J(1 + \cot \phi_1) \mp h_z$	2	$ \pm 1,2\rangle = \left\{ \frac{\sqrt{2}}{2} \sin \phi_1 \left(\begin{pmatrix} 0 \\ 0 \\ \pm 1 \end{pmatrix} - \begin{pmatrix} 0 \\ 0 \\ \pm 1 \end{pmatrix} \right) + \cos \phi_1 \left(\begin{pmatrix} \pm 1 \\ \pm 1 \\ \mp 1 \end{pmatrix} - \begin{pmatrix} \mp 1 \\ \mp 1 \\ \pm 1 \end{pmatrix} \right) \right.$ $\left. \frac{\sqrt{6}}{6} \cos \phi_1 \left(2 \begin{pmatrix} \pm 1 \\ \pm 1 \\ \mp 1 \end{pmatrix} - \begin{pmatrix} \pm 1 \\ \mp 1 \\ \pm 1 \end{pmatrix} - \begin{pmatrix} \mp 1 \\ \pm 1 \\ \pm 1 \end{pmatrix} \right) + \sin \phi_1 \left(2 \begin{pmatrix} \pm 1 \\ 0 \\ 0 \end{pmatrix} - \begin{pmatrix} 0 \\ \pm 1 \\ 0 \end{pmatrix} - \begin{pmatrix} 0 \\ 0 \\ \pm 1 \end{pmatrix} \right) \right\}$
	10			
11	$J(1 - \tan \phi_1) \mp h_z$	2	$ \pm 1,3\rangle = \left\{ \frac{\sqrt{2}}{2} \cos \phi_1 \left(\begin{pmatrix} \pm 1 \\ 0 \\ 0 \end{pmatrix} - \begin{pmatrix} 0 \\ \pm 1 \\ 0 \end{pmatrix} \right) + \sin \phi_1 \left(\begin{pmatrix} \pm 1 \\ \pm 1 \\ \mp 1 \end{pmatrix} - \begin{pmatrix} \mp 1 \\ \mp 1 \\ \pm 1 \end{pmatrix} \right) \right.$ $\left. \frac{\sqrt{6}}{6} \sin \phi_1 \left(2 \begin{pmatrix} \pm 1 \\ \pm 1 \\ \mp 1 \end{pmatrix} - \begin{pmatrix} \pm 1 \\ \mp 1 \\ \pm 1 \end{pmatrix} - \begin{pmatrix} \mp 1 \\ \pm 1 \\ \pm 1 \end{pmatrix} \right) - \cos \phi_1 \left(2 \begin{pmatrix} 0 \\ 0 \\ \pm 1 \end{pmatrix} - \begin{pmatrix} 0 \\ \pm 1 \\ 0 \end{pmatrix} - \begin{pmatrix} 0 \\ 0 \\ \pm 1 \end{pmatrix} \right) \right\}$	
12				
2	13	$J - J_z \mp 2h_z$	2	$ \pm 2,0\rangle = \left\{ \frac{\sqrt{2}}{2} \left(\begin{pmatrix} \pm 1 \\ \pm 1 \\ 0 \end{pmatrix} - \begin{pmatrix} 0 \\ \pm 1 \\ \pm 1 \end{pmatrix} \right) \right.$ $\left. \frac{\sqrt{6}}{6} \left(\begin{pmatrix} \pm 1 \\ \pm 1 \\ 0 \end{pmatrix} - 2 \begin{pmatrix} \pm 1 \\ 0 \\ \pm 1 \end{pmatrix} + \begin{pmatrix} 0 \\ \pm 1 \\ \pm 1 \end{pmatrix} \right) \right\}$
	14			
3	15	$-2J - J_z \mp 2h_z$	1	$ \pm 2,1\rangle = \frac{\sqrt{3}}{3} \left(\begin{pmatrix} \pm 1 \\ \pm 1 \\ 0 \end{pmatrix} + \begin{pmatrix} \pm 1 \\ 0 \\ \pm 1 \end{pmatrix} + \begin{pmatrix} 0 \\ \pm 1 \\ \pm 1 \end{pmatrix} \right)$
	16			
3	17	$-3J_z \mp 3h_z$	1	$ \pm 3,0\rangle = \begin{pmatrix} \pm 1 \\ \pm 1 \\ \pm 1 \end{pmatrix}$
	18			

A. Ground-state phase diagram

The ground-state phase diagram shown in Fig. 2(a) totally involves seven phases specified below. First, the saturated paramagnetic phase (SA) has according to Eq. (3) the following energy per unit cell

$$E_{SA} = -3J_0 - 3J_z - 3h_z - \frac{1}{2}h, \quad (4)$$

which corresponds to the eigenstate defined through the eigenvector $|3,0\rangle_i$ specified in Table I

$$|SA\rangle = \prod_{i=1}^N |3,0\rangle_i |+\rangle_i. \quad (5)$$

Obviously, both Ising spin magnetization per unit cell ($m_I = \frac{1}{2}$) and Heisenberg spin magnetization per unit cell

($m_H = 3$) are fully polarized, and total magnetization per unit cell attains the following value $m_t = m_I + m_H = \frac{7}{2}$.

The ground-state phase diagram shown in Fig. 2(a) also displays three different ferrimagnetic (FI) phases. The ground-state energy of the first ferrimagnetic phase FI_1 reads

$$E_{FI_1} = 2J + J_z - \frac{1}{2}h, \quad (6)$$

whereas its corresponding eigenvector is given by

$$|FI_1\rangle = \prod_{i=1}^N |0,4\rangle_i |+\rangle_i \quad (7)$$

with the eigenvector $|0,4\rangle_i$ defined in Table I. In the first ferrimagnetic phase FI_1 the Ising spin magnetization is

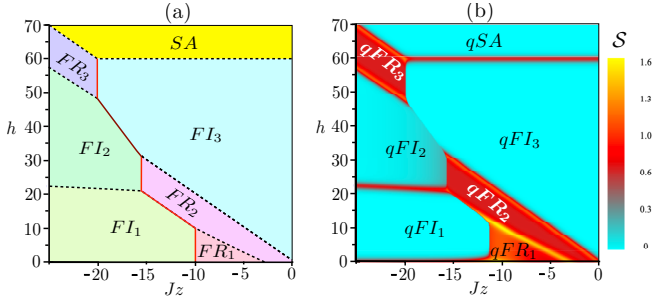


Figure 2: (a) Ground-state phase diagram in the $J_z - h$ plane by assuming the fixed parameters $J = -10$, $J_0 = -10$, and $h_z = h$; (b) Density-plot of entropy in the $J_z - h$ plane for the same set of parameters as in (a) at $T = 0.4$.

$m_I = \frac{1}{2}$, the Heisenberg spin magnetization equals zero $m_H = 0$, and the total magnetization thus becomes $m_t = \frac{1}{2}$.

The ground-state energy for the second ferrimagnetic phase FI_2 can be expressed as

$$E_{FI_2} = -J_0 - 2J(1 - \cot \phi_2) - h_z - \frac{1}{2}h, \quad (8)$$

where $\cot(2\phi_2) = \frac{J_z + 2J}{4J}$ with $-\frac{\pi}{4} < \phi_2 < \frac{\pi}{4}$. The corresponding eigenvector reads

$$|FI_2\rangle = \prod_{i=1}^N |1, 1\rangle_i |+\rangle_i \quad (9)$$

with the eigenvector $|1, 1\rangle_i$ defined in Table I. The Ising spin magnetization in the second ferrimagnetic phase FI_2 becomes $m_I = \frac{1}{2}$, the Heisenberg spin magnetization is $m_H = 1$, and the total magnetization is $m_t = \frac{3}{2}$.

The ground-state energy for the third ferrimagnetic phase FI_3 is given by

$$E_{FI_3} = 3J_0 - 3J_z - 3h_z + \frac{1}{2}h, \quad (10)$$

whereas its corresponding eigenvector reads

$$|FI_3\rangle = \prod_{i=1}^N |3, 0\rangle_i |-\rangle_i \quad (11)$$

with the eigenvector $|3, 0\rangle_i$ being defined in Table I. Analogously to the previous case, the Ising spin magnetization is given by $m_I = -\frac{1}{2}$, the Heisenberg spin magnetization equals to $m_H = 3$, and the total magnetization is $m_t = \frac{5}{2}$. It should be pointed out that the saturated paramagnetic phase as well as all three ferrimagnetic phases are non-degenerate, which means that there is no residual entropy $S = 0$ at zero temperature within those ground states.

However, the ground state of the mixed spin-(1/2, 1) Ising-Heisenberg double-tetrahedral chain may be one of three frustrated (FR) phases with a nonzero residual entropy. The ground-state energy of the first frustrated phase FR_1 is given by

$$E_{FR_1} = J_0 - J(1 + \cot \phi_1) - h_z + \frac{1}{2}h, \quad (12)$$

where $\cot(2\phi_1) = \frac{J_z - J}{2J}$ with $-\frac{\pi}{4} < \phi_1 < \frac{\pi}{4}$. The corresponding ground-state eigenvector reads as follows

$$|FR_1\rangle = \prod_{i=1}^N |1, 3\rangle_i |-\rangle_i, \quad (13)$$

where two-fold degenerate eigenstate $|1, 3\rangle_i$ is specified in Table I. Owing to this fact, the frustrated phase FR_1 is macroscopically degenerate with the residual entropy $S = \ln(2)$ per unit cell when the entropy is measured in units of the Boltzmann constant k_B . Note that the Ising spin magnetization is being $m_I = -\frac{1}{2}$, the Heisenberg spin magnetization is $m_H = 1$, and the total magnetization becomes $m_t = \frac{1}{2}$.

The ground-state energy of the second frustrated phase FR_2 can be expressed as follows

$$E_{FR_2} = 2J_0 + J - J_z - 2h_z + \frac{1}{2}h \quad (14)$$

and its respective eigenvector is given by

$$|FR_2\rangle = \prod_{i=1}^N |2, 0\rangle_i |-\rangle_i. \quad (15)$$

The definition of two-fold degenerate eigenstate $|2, 0\rangle_i$ is reported in Table I, which implies that the second frustrated phase FR_2 also has residual entropy $S = \ln(2)$. The Ising spin magnetization is $m_I = -\frac{1}{2}$, the Heisenberg spin magnetization is $m_H = 2$, and the total magnetization results in $m_t = \frac{3}{2}$.

The ground-state energy of the third frustrated phase FR_3 follows from the relation

$$E_{FR_3} = -2J_0 + J - J_z - 2h_z - \frac{1}{2}h, \quad (16)$$

whereas its respective eigenvector reads

$$|FR_3\rangle = \prod_{i=1}^N |2, 0\rangle_i |+\rangle_i. \quad (17)$$

The two-fold degenerate eigenvector $|2, 0\rangle_i$ is defined in Table I and hence, the third frustrated phase FR_2 is macroscopically degenerate with the residual entropy $S = \ln(2)$ per unit cell. The corresponding Ising spin magnetization achieves the value $m_I = \frac{1}{2}$, the Heisenberg spin magnetization equals to $m_H = 2$, and the total magnetization is given by $m_t = \frac{5}{2}$.

Usually, plots can be drawn in units of some parameters like J , and then the temperature can be measured in units J . However, here for convenience, we set the parameters to be $J = -10$ and $J_0 = -10$, just for scale the temperature by a factor 10. From now on, we will consider this set of parameters to study the pseudo-critical temperature throughout the article.

All dashed lines in Fig. 2(a) represent usual ground-state phase boundaries between two phases. The residual entropy per unit cell at the phase boundary between FR_1 and FR_2 becomes $S = \ln(4)$. Similarly, the residual

entropy at the interface between FR_2 and FI_3 equals to $\mathcal{S} = \ln(3)$, while the residual entropy at the phase boundary between FI_3 and SA equals to $\mathcal{S} = \ln(2)$. Analogously, the residual entropy attains the value $\mathcal{S} = \ln(3)$ at phase boundaries between $SA - FR_3$ and $FR_3 - FI_2$. Finally, the residual entropy becomes $\mathcal{S} = \ln(2)$ at the interface between FI_2 and FI_3 . In all aforementioned cases the residual entropy per unit cell is always higher than the entropy of both individual phases, which coexist together at a relevant ground-state boundary. By contrast, solid lines represent all unusual phase boundaries between two phases. The residual entropy per unit cell $\mathcal{S} = \ln(2)$ can be found at interfaces between the phases FR_1-FI_1 , FR_2-FI_1 , FR_2-FI_2 , and FR_3-FI_3 , whereas the residual entropy per unit cell vanishes $\mathcal{S} = 0$ at the interface between two non-degenerate ferrimagnetic phases FI_2 and FI_3 .

III. THERMODYNAMICS

The mixed spin-(1/2,1) Ising-Heisenberg double-tetrahedral chain can be mapped onto the effective spin-1/2 Ising chain given by the Hamiltonian

$$H = - \sum_{i=1}^N [K_0 + K s_i s_{i+1} + \frac{1}{2} B (s_i + s_{i+1})], \quad (18)$$

where K_0 , K , and B are effective temperature-dependent parameters. Bearing this in mind, thermodynamics of the effective spin-1/2 Ising chain can be expressed in terms of the transfer matrix $\mathbf{V} = \begin{bmatrix} w_1 & w_0 \\ w_0 & w_{-1} \end{bmatrix}$ according to the procedure previously discussed in Ref. [17]. Each element of the transfer matrix (Boltzmann factor) w_n with $n = \{-1, 0, 1\}$, which will be further referred to as the sector, can be defined as

$$w_n = \sum_{k=0}^{18} g_{n,k} e^{-\beta \varepsilon_{n,k}}, \quad (19)$$

where $\beta = 1/(k_B T)$, k_B is Boltzmann's constant, T is the absolute temperature and the eigenvalues $\varepsilon_{n,k}$ are given by Eq. (3).

To be more specific, the Boltzmann factors are explicitly given by

$$w_n = u^n \left\{ q_{3,n} z^6 + \left(x^4 + \frac{2}{x^2} \right) z^2 q_{2,n} + \frac{(2t + x^{-4})}{z^2} + \frac{1}{z} \left[\left(\frac{2y_1}{x} + x^2 y_2 \right) q_{1,n} + x^2 y_3 \right] \right\}, \quad (20)$$

where $x = e^{\beta J/2}$, $z = e^{\beta J_z/2}$, $u = e^{\beta h/2}$, $t = 2 \cosh(\beta J)$, while the coefficients y_r and $q_{r,n}$ with $r = \{1, 2, 3\}$ are defined as follows

$$y_r = 2 \cosh[\beta J \csc(2\phi_r)], \quad (21)$$

$$q_{r,n} = 2 \cosh[r\beta(nJ_0 + h_z)]. \quad (22)$$

The transfer-matrix eigenvalues are determined by the following equation

$$\lambda_{\pm} = \frac{1}{2} \left(w_1 + w_{-1} \pm \sqrt{(w_1 - w_{-1})^2 + 4w_0^2} \right). \quad (23)$$

Considering the effective spin-1/2 Ising chain under a periodic boundary condition gives the partition function $\mathcal{Z}_N = \lambda_+^N + \lambda_-^N$. Consequently, the free energy can be obtained in the thermodynamic limit ($N \rightarrow \infty$) according to the formula

$$f = -\frac{1}{\beta} \ln \left[\frac{1}{2} \left(w_1 + w_{-1} + \sqrt{(w_1 - w_{-1})^2 + 4w_0^2} \right) \right]. \quad (24)$$

Substituting Boltzmann's factors w_n into Eq. (24), we can exactly calculate the free energy of the mixed spin-(1/2,1) Ising-Heisenberg double-tetrahedral chain at finite temperature.

It has been recently demonstrated [17] that some 1D lattice-statistical models satisfy the following condition $|w_1 - w_{-1}| \gg w_0$ at low enough temperatures. Under this condition, the free energy of the mixed spin-(1/2,1) Ising-Heisenberg double-tetrahedral chain reduces to

$$f = -T \ln \{ \max [w_1(T), w_{-1}(T)] \}. \quad (25)$$

The final formula for the free energy per unit cell (24) takes the following simple form at a phase boundary between the individual phases with the same energy ε_c

$$f = \varepsilon_c - T \ln [\max (g_{1,0}, g_{-1,0})]. \quad (26)$$

Consequently, the residual entropy per unit cell at a relevant phase boundary reads

$$\mathcal{S}_c = \ln [\max (g_{1,0}, g_{-1,0})]. \quad (27)$$

Knowing this quantity is sufficient for prediction of a pseudo-transition at finite temperatures [18].

In Fig. 2(b) we illustrate the density plot of the entropy as a function of J_z and h for the fixed temperature $T = 0.4$ by using the same scale as in the ground-state phase diagram shown in Fig. 2(a). It is quite evident that the entropy follows the vestige of zero-temperature phase diagram at finite temperatures. The notation for the ground state is changed at finite temperatures by adding a prefix "q" to the name of respective ground states, which will denote the respective quasi-phase [8] because of a lack of true spontaneous long-range order at finite temperatures. It could be expected that thermal excitations basically influence the phase boundaries. It has been argued previously that all dashed curves displayed in Fig. 2(a) describe standard interfaces, which are manifested through an increase of the entropy exceeding the entropy value of both coexisting phases. Contrary to this, the phase boundaries depicted by solid lines in Fig. 2(a) behave quite differently, since they show at the respective interface a sharp rise of the entropy to a greater entropy of one of two coexisting phases.

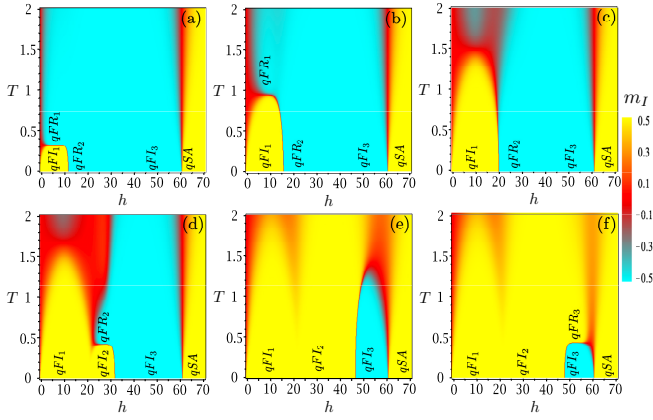


Figure 3: Density plot of Ising spin magnetization in the $T - h$ plane for the fixed values of the coupling constants $J = -10$, $J_0 = -10$, and several values of J_z : (a) $J_z = -11$; (b) $J_z = -13$; (c) $J_z = -15$; (d) $J_z = -15.65$; (e) $J_z = -19$; (f) $J_z = -19.85$.

The density plot of Ising spin magnetization is depicted in Fig. 3 in the $T - J_z$ plane for the following set of parameters $J = -10$ and $J_0 = -10$. In this figure, yellow region corresponds to spin 'up' ($m_I = 1/2$), cyan region corresponds to spin 'down' ($m_I = -1/2$), and red region corresponds to null Ising magnetization ($m_I = 0$). Surely the temperature in units of $T/|J|$ would be divided by a factor 10 in Fig. 3 and the following figures.

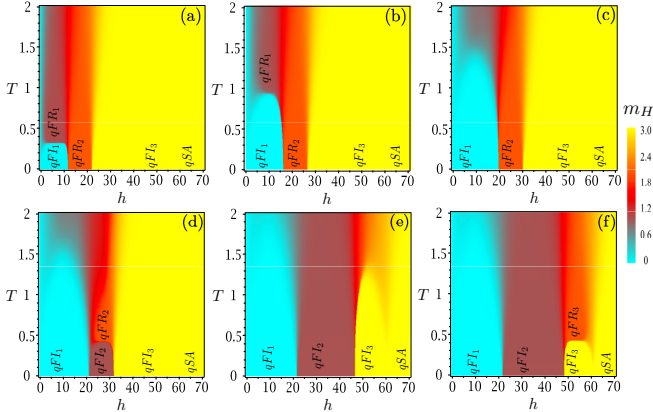


Figure 4: Density plot of Heisenberg spin magnetization in the $T - h$ plane for the fixed values of the coupling constants $J = -10$, $J_0 = -10$, and several values of J_z : (a) $J_z = -11$; (b) $J_z = -13$; (c) $J_z = -15$; (d) $J_z = -15.65$; (e) $J_z = -19$; (f) $J_z = -19.85$.

The density plot of the Heisenberg spin magnetization is depicted in Fig. 4 in the $T - J_z$ plane for the same set of parameters $J = -10$ and $J_0 = -10$. The color code for the density plot is as follows: yellow region corresponds to the saturated Heisenberg magnetization $m_H = 3$, cyan region corresponds to the null Heisenberg magnetization $m_H = 0$, orange region corresponds to the moderate Heisenberg magnetization $m_H = 2$, and dark

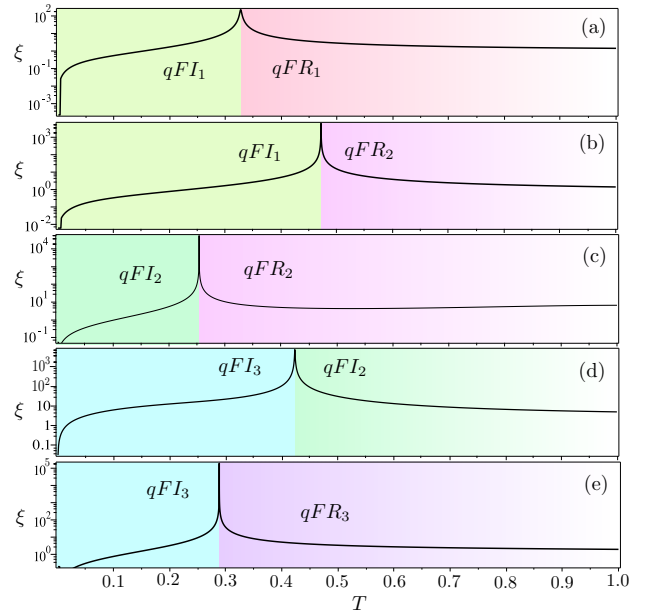


Figure 5: Correlation length against temperature for the fixed parameters $J = -10$, $J_0 = -10$ and several values of J_z and $h_z = h$: (a) $h = 4$, $J_z = -11$; (b) $h = 11$, $J_z = -11.5$; (c) $h = 26$, $J_z = -15.6$; (d) $h = 36.76$, $J_z = -17$; (e) $h = 52$, $J_z = -19.9$.

red region corresponds to the moderate Heisenberg magnetization $m_H = 1$. It can be seen from Figs. 3 and 4 that the pseudo-transitions between the quasi-phases is accompanied with abrupt change in the magnetization of the Ising spins and/or the magnetization of the Heisenberg spins. The density plots shown in Fig. 4(a)-(f) imply a full alignment of the Heisenberg spins just within the quasi-phases qFI_3 and qSA .

Now, let us analyze the correlation length, which can be calculated according to the following simple relation

$$\xi = \left[\ln \left(\frac{\lambda_+}{\lambda_-} \right) \right]^{-1}. \quad (28)$$

The correlation length is depicted in Fig. 5 as a function of temperature for the fixed parameters $J = -10$, $J_0 = -10$, and $h_z = h$. It is advisable to follow the zero-temperature phase diagram to interpret the relevant dependences of the correlation length. In Fig. 5(a) we illustrate the correlation length for $h = 4$ and $J_z = -11$, whereas the shark peak delimits the quasi-phases qFI_1 and qFR_1 in agreement with the ground-state phase diagram shown in Fig. 2(a). Although the correlation length seems to diverge at a pseudo-critical temperature, it is in fact just a sharp finite peak. In Fig. 5(b) one observes a similar curve for $h = 11$ and $J_z = -11.5$, but now the peak indicates a pseudo-transition between the quasi-phases qFI_1 and qFR_2 . Fig. 5(c) depicts the correlation length for $h = 30$ and $J_z = -15.65$, whereas the sharp peak determines a pseudo-transition between the quasi-phases qFI_2 and qFR_2 . Similarly, the correlation length plotted in Fig. 5(d)-(e) demonstrates that

a pseudo-transition between the quasi-phases qFI_3 - qFI_2 and qFI_3 - qFR_3 are accompanied with a sharp robust peak of the correlation length. It is worthy to mention that the quasi-phases melt smoothly upon increasing temperature when the temperature is higher than the pseudo-critical temperature.

It is quite clear from Eq. (25) that the pseudo-critical temperature T_p can be alternatively obtained by solving the equation

$$w_1(T_p) = w_{-1}(T_p). \quad (29)$$

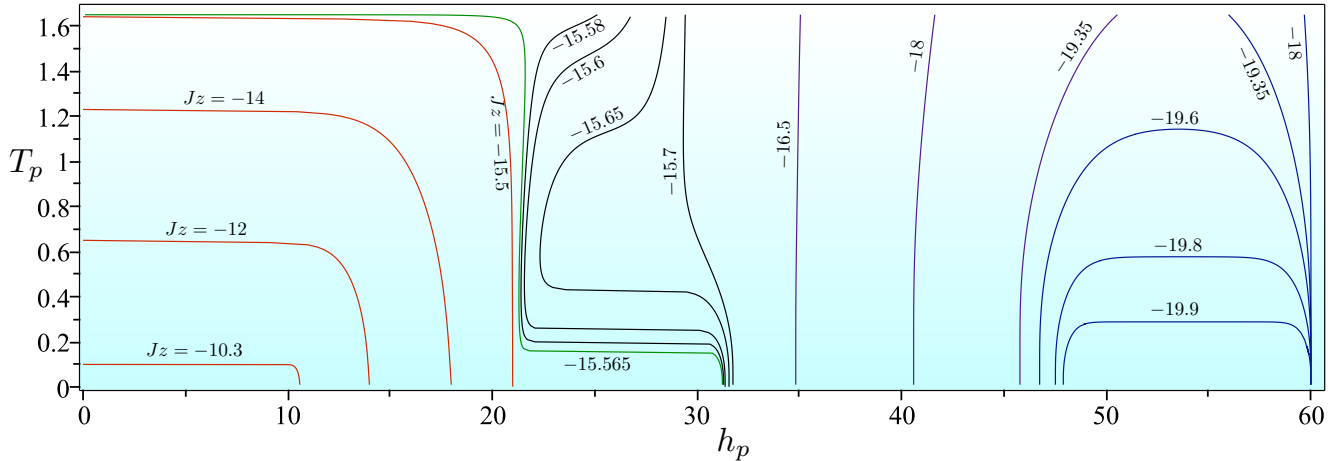


Figure 6: Pseudo-critical temperature as a function of the magnetic field for the fixed values of interaction parameters $J = -10$, $J_0 = -10$, $h_z = h$ and several values of J_z .

The numerical solution of Eq. (29) allows us to plot the pseudo-critical temperature T_p against the magnetic field h_p for several values of J_z (see Fig. 6). For sufficiently low magnetic fields $0 < h_p < 10$ the pseudo-critical temperature delimits the quasi-phases qFI_1 (below the curve) and qFR_1 (above the curve), whereas for the moderate fields $10 \lesssim h_p \lesssim 21$ the pseudo-transition line delimits the quasi-phases qFI_1 (left from the curve) and qFR_2 (right from the curve). Furthermore, the investigated model undergoes a pseudo-transition between the quasi-phases qFI_2 and qFR_2 for $T_p \lesssim 0.6$ and $21 \lesssim h_p \lesssim 31$, while the pseudo-transition between the quasi-phases qFI_2 (left side of the curve) and qFI_3 (right side of the curve) takes place for $31 \lesssim h_p \lesssim 51$. Finally, the pseudo-transition line delimits the quasi-phases qFI_3 (below the curve) and qFR_3 (above the curve) for high enough magnetic fields $51 \lesssim h_p < 60$. Although the condition (29) may still give relatively high values of the pseudo-critical temperature (e.g., $T \gtrsim 1$), it turns out that the pseudo-critical line melts smoothly for sufficiently high temperatures $T \sim 1$ (in some particular cases even at lower temperatures). In general, there is no way to identify the maximum value of the pseudo-critical temperature. Besides, the pseudo-critical temperature also melts for $h_p \rightarrow 0$ and $h_p \rightarrow 60$ as evidenced by Figs. 3 and 4.

Temperature variations of some thermodynamic quantities are plotted in Fig. 7 close to a pseudo-transition

between the quasi-phases qFR_1 and qFI_1 for the fixed values of the interaction parameters $J = -10$, $J_0 = -10$, $J_z = -11$, and several values of the magnetic field $h = \{4, 6, 8, 9, 10\}$ outlined by {black solid, orange solid, red solid, blue dashed, and green dot dashed} curves, respectively. A strong thermally-induced change of the entropy $\mathcal{S}(T)$ is observable in Fig. 7(a) around the pseudo-critical temperature $T_p \approx 0.3275$. It is worthy to mention that the pseudo-critical temperature remains almost constant for $0 < h < 10$. It is quite evident from Fig. 7(b), moreover, that the Ising spins are mostly aligned parallel to the magnetic field ($m_I = 0.5$) below the pseudo-critical temperature $T < T_p$ and antiparallel ($m_I = -0.5$) above it $T > T_p$. Contrary to this, the Heisenberg spins almost do not contribute to the total magnetization ($m_H = 0$) below the pseudo-critical temperature $T < T_p$, while they provide a significant contribution ($m_H = 1$) above it $T > T_p$. Last but not least, the specific heat and magnetic susceptibility displayed in Fig. 7(d)-(e) in a semi-logarithmic scale serve in evidence of a pseudo-transition through a strong narrow peak observable at the pseudo-critical temperature.

Temperature dependences of selected thermodynamic quantities are depicted in Fig. 8 by assuming the fixed values of the interaction parameters $J = -10$, $J_0 = -10$, and $(h, J_z) = \{(11, -11.5), (13, -12), (15.5, -13), (16.9, 13.6), (18.81, -14.5)\}$ outlined by {black solid, or-

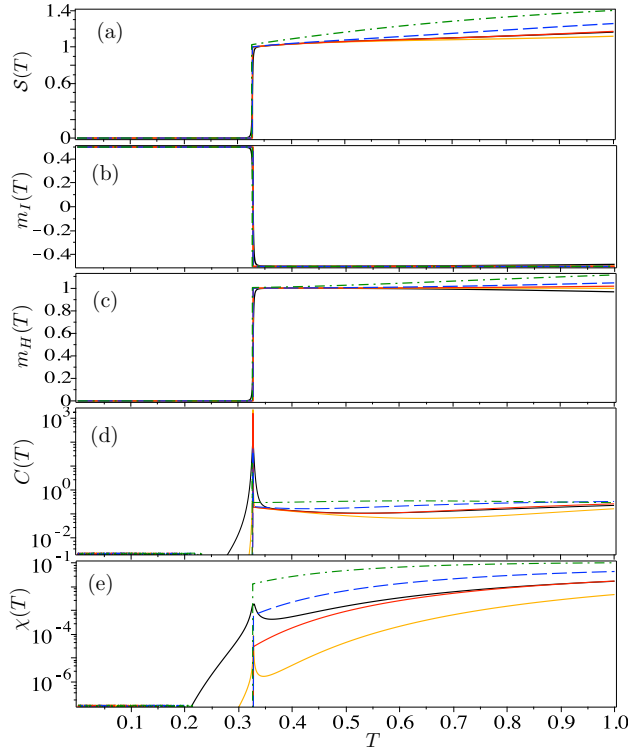


Figure 7: Temperature dependences of some thermodynamic quantities by considering the fixed parameters $J = -10$, $J_0 = -10$, $J_z = -11$, and several values of the magnetic field $h = \{4, 6, 8, 9, 10\}$ (black solid, orange solid, red solid, blue dashed, and green dot dashed): (a) entropy \mathcal{S} ; (b) Ising spin magnetization; (c) Heisenberg spin magnetization; (d) specific heat (semi-logarithmic plot); (e) magnetic susceptibility (semi-logarithmic plot).

ange solid, red solid, blue dashed, and green dot dashed} curves, respectively. The present choice of the interaction parameters is consistent with the pseudo-transition between the quasi-phases qFI_1 and qFR_2 , which varies with the interaction parameter J_z and magnetic field h . It is obvious from Fig. 8(a) that the entropy $\mathcal{S}(T)$ exhibits a steep increase close to a pseudo-critical temperature T_p , while the magnetization of Ising spins shown in Fig. 8(b) is pointing upward ($m_I = 0.5$) for $T < T_p$ and downward ($m_I = -0.5$) for $T > T_p$. Similarly, the magnetization of Heisenberg spins illustrated in Fig. 8(c) is zero ($m_H = 0$) for $T < T_p$, while there is a sudden change at $T = T_p$ above which it strongly depends on the magnetic field h and the coupling constant J_z . Finally, sharp narrow peaks can be repeatedly detected at a pseudo-critical temperature in the respective temperature dependences of the specific heat [Fig. 8(d)] and the magnetic susceptibility [Fig. 8(e)].

A pseudo-transition between the quasi-phases qFI_2 and qFR_2 is illustrated in Fig. 9 by considering the fixed parameters $J = -10$, $J_0 = -10$, $J_z = -15.65$, and several values of the magnetic field of $h = \{25, 27, 28, 29, 30\}$ outlined by {black solid, orange solid, red solid, blue

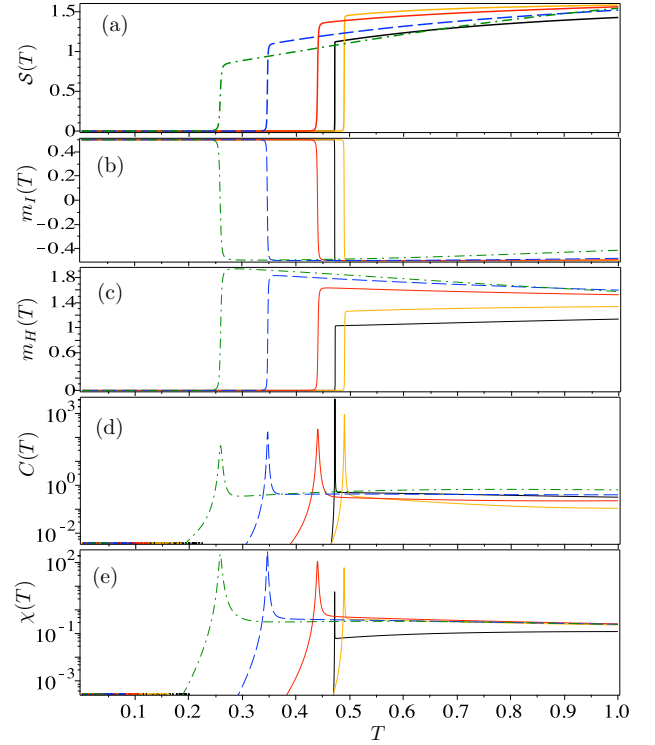


Figure 8: Temperature dependences of some thermodynamic quantities by considering the fixed parameters $J = -10$, $J_0 = -10$, and $(h, J_z) = \{(11, -11.5), (13, -12), (15.5, -13), (16.9, 13.6), (18.81, -14.5)\}$ (black solid, orange solid, red solid, blue dashed, and green dot dashed): (a) entropy \mathcal{S} ; (b) Ising spin magnetization; (c) Heisenberg spin magnetization; (d) specific heat (semi-logarithmic plot); (e) magnetic susceptibility (semi-logarithmic plot).

dashed, and green dot dashed} curves, respectively. Fig. 9(a) shows the entropy $\mathcal{S}(T)$ as a function of temperature: for $T < T_p$ the entropy increases significantly but is virtually independent of h (for $22 \lesssim h \lesssim 30$), then a sudden rise occurs at $T = T_p$ followed by a successive smooth increase for $T > T_p$. The Ising magnetization depicted in Fig. 9(b) is nearly constant $m_I = 0.5$ for $T < T_p$, but it becomes almost -0.5 for $T \gtrsim T_p$ before showing a continuous rise approaching null upon further increase of temperature. Analogously, the Heisenberg spin magnetization illustrated in Fig. 9(c) tends to zero $m_H \rightarrow 1$ for $T < T_p$, while it approaches to $m_H \rightarrow 2$ for $T \gtrsim T_p$. The specific heat and magnetic susceptibility plotted in Fig. 9(d)-(e) in a semi-logarithmic scale display vigorous narrow peaks verifying a pseudo-transition between the quasi-phases qFI_2 and qFR_2 .

Next, the pseudo-transition at the interface between the quasi-phases qFI_2 and qFI_3 is illustrated in Fig. 10 by considering set of the parameters $J = -10$, $J_0 = -10$, and $(h, J_z) = \{(36.76, -17), (38.7, -17.5), (40.6, -18), (42.55, 18.5), (44.45, -19)\}$ drawn by {black solid, orange solid, red solid, blue dashed, and green dot dashed} curves, respectively. It should be stressed that both coexisting quasi-phases qFI_2 and qFI_3 are non-frustrated and

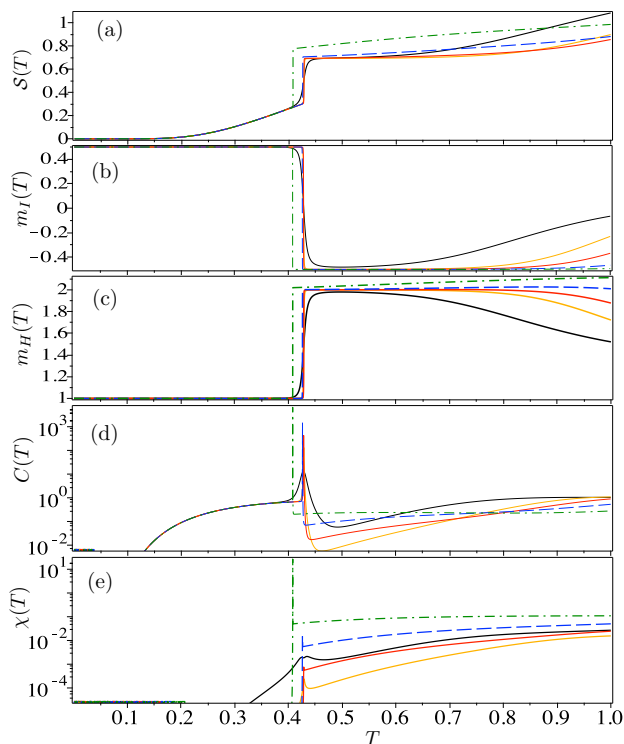


Figure 9: Temperature dependences of some thermodynamic quantities by considering the fixed parameters $J = -10$, $J_0 = -10$, $J_z = -15.65$, and several values of the magnetic field $h = \{25, 27, 28, 29, 30\}$ (black solid, orange solid, red solid, blue dashed, and green dot dashed): (a) entropy \mathcal{S} ; (b) Ising spin magnetization; (c) Heisenberg spin magnetization; (d) specific heat (semi-logarithmic plot); (e) magnetic susceptibility (semi-logarithmic plot).

consequently, the residual entropy per unit cell should also become null according to Eq. (27). The entropy $\mathcal{S}(T)$ as a function of temperature shown in Fig. 10(a) is for $T < T_p$ nearly zero, then it shows a small but sudden rise at $T = T_p$, which is followed by a roughly linear increase for $T > T_p$. The magnetization of Ising spins [Fig. 10(b)] displays an opposite behavior to the previous one: the Ising spins are aligned in opposite to the magnetic field ($m_I = -0.5$) for $T < T_p$ and they are aligned in the magnetic-field direction ($m_I = 0.5$) for $T > T_p$. Similarly, the magnetization of Heisenberg spins [Fig. 10(c)] is close to its maximal value $m_H = 3$ for $T < T_p$ and it suddenly drops to $m_H = 1$ for $T > T_p$. Finally, one observes a typical narrow peak in thermal variations of the specific heat and magnetic susceptibility displayed in Fig. 10(d)-(e).

Last but not least, let us discuss a pseudo-transition between the quasi-phases qFR_3 and qFI_3 exemplified in Fig. 11 for the fixed values of the interaction parameters $J = -10$, $J_0 = -10$, $J_z = -19.9$, and several magnetic fields $h = \{50, 52, 54, 56, 56.5\}$ sketched by {black solid, orange solid, red solid, blue dashed, and green dot dashed} curves, respectively. It is noteworthy that thermal variation of the entropy $\mathcal{S}(T)$ displayed in Fig. 11(a)

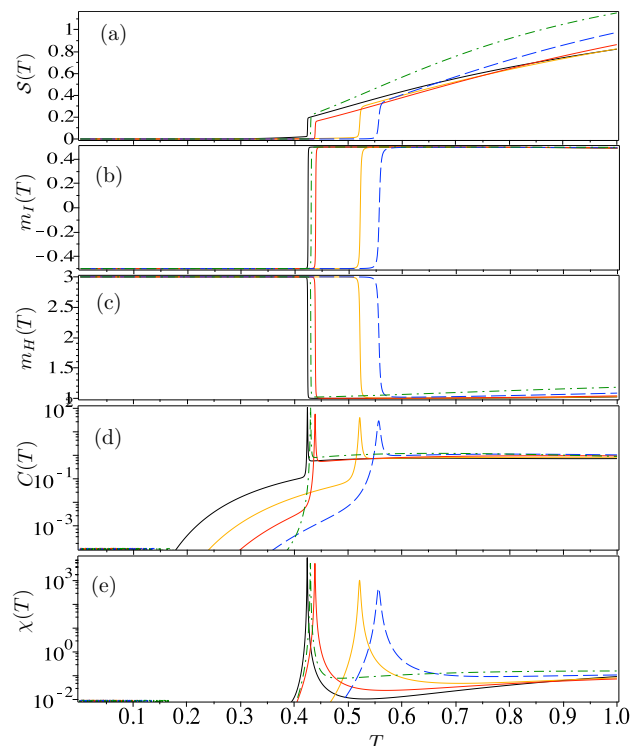


Figure 10: Temperature dependences of some thermodynamic quantities by considering the fixed parameters $J = -10$, $J_0 = -10$, and $(h, J_z) = \{(36.76, -17), (38.7, -17.5), (40.6, -18), (42.55, 18.5), (44.45, -19)\}$ (black solid, orange solid, red solid, blue dashed, and green dot dashed): (a) entropy \mathcal{S} ; (b) Ising spin magnetization; (c) Heisenberg spin magnetization; (d) specific heat (semi-logarithmic plot); (e) magnetic susceptibility (semi-logarithmic plot).

is quite reminiscent of the entropy dependence illustrated in Fig. 7(a). In addition, the temperature dependences of the magnetization of the Ising and Heisenberg spins shown in Fig. 11(b) and (c) are quite similar to the previous cases shown in Fig. 10(b) and (c), respectively. Although the specific heat shows a strong narrow peak at the pseudo-critical temperature, it often becomes negligible further away from the pseudo-critical temperature [see Fig. 11(d)]. The similar situation can be also found in the temperature dependences of the magnetic susceptibility shown in Fig. 11(e).

IV. CONCLUSIONS

The pseudo-transitions of the mixed spin-(1/2,1) Ising-Heisenberg double-tetrahedral chain are examined in detail at non-zero temperature and magnetic field. The ground-state phase diagram of the investigated spin chain totally involves seven phases, three of which can be classified as the non-degenerate ferrimagnetic phases, three as the macroscopically degenerate frustrated phases, and one as the saturated paramagnetic phase. Interestingly, five different ground-state boundaries of the mixed spin-

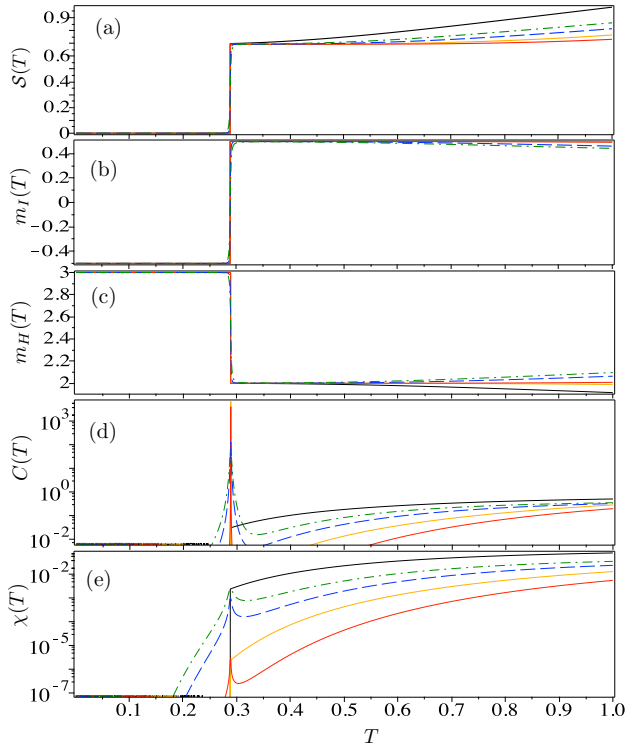


Figure 11: Temperature dependences of some thermodynamic quantities by considering the fixed parameters $J = -10$, $J_0 = -10$, $J_z = -19.9$, and several values of the magnetic field $h = \{50, 52, 54, 56, 56.5\}$ (black solid, orange solid, red solid, blue dashed, and green dot dashed): (a) entropy \mathcal{S} ; (b) Ising spin magnetization; (c) Heisenberg spin magnetization; (d) specific heat (semi-logarithmic plot); (e) magnetic susceptibility (semi-logarithmic plot).

(1/2,1) Ising-Heisenberg double-tetrahedral chain represent peculiar interfaces, at which the residual entropy per unit cell is simply given by the larger entropy of one of two coexisting phases. This condition seems to be sufficient criterion whether or not the pseudo-transition does emerge in a close vicinity of the ground-state phase boundary. In fact, the residual entropy per unit cell at the usual ground-state phase boundaries is strictly larger than the residual entropy of both coexisting phases. Although thermal fluctuations usually destroy in 1D lattice-statistical models with short-range interactions all fingerprints of the ground-state phase boundaries, the aforementioned five interfaces are quite robust with respect to thermal fluctuations. In consequence of that, the mixed spin-(1/2,1) Ising-Heisenberg double-tetrahedral chain may exhibit in a vicinity of five aforementioned ground-state phase boundaries a marked pseudo-transition manifested by vigorous narrow peaks of the specific heat and magnetic susceptibility besides a sudden change of the entropy and magnetization.

Acknowledgments

This work was partially supported by Brazilian Agency CNPq and FAPEMIG.

-
- [1] J. F. Nagle, *Am. J. Phys.* **36**, 1114 (1968).
 - [2] C. Kittel, *Am. J. Phys.* **37**, 917 (1969).
 - [3] S. T. Chui and J. D. Weeks, *Phys. Rev. B* **23**, 2438 (1981).
 - [4] T. Dauxois and M. Peyrard, *Phys. Rev. E* **51**, 4027 (1995).
 - [5] P. Sarkanych, Y. Holovatch, and R. Kenna, *Phys. Lett. A* **381**, 3589 (2017).
 - [6] L. van Hove, *Physica* **16**, 137 (1950).
 - [7] J. A. Cuesta and A. Sanchez, *J. Stat. Phys.* **115**, 869 (2003).
 - [8] P. N. Timonin, *J. Exp. Theor. Phys.* **113**, 251 (2011).
 - [9] I. M. Carvalho, J. Torrico, S. M. de Souza, M. Rojas, and O. Rojas, *J. Magn. Magn. Mater.* **465**, 323 (2018).
 - [10] I. M. Carvalho, J. Torrico, S. M. de Souza, O. Rojas, and O. Derzhko, *Ann. Phys.* **402**, 45 (2019).
 - [11] O. Rojas, J. Strečka, and S. M. de Souza, *Solid State Commun.* **246**, 68 (2016).
 - [12] J. Strečka, R. C. Alecio, M. Lyra, and O. Rojas, *J. Magn. Magn. Mater.* **409**, 124 (2016).
 - [13] J. Strečka, arXiv:1904.10704.
 - [14] L. Gálisová and J. Strečka, *Phys. Rev. E* **91**, 0222134 (2015).
 - [15] L. Gálisová, *Phys. Rev. E* **96**, 052110 (2017).
 - [16] L. Gálisová and D. Knežo, *Phys. Lett. A* **382**, 2839 (2018).
 - [17] S. M. de Souza and O. Rojas, *Solid State Commun.* **269**, 131 (2017).
 - [18] O. Rojas, arXiv:1810.07817.
 - [19] T. Krokhmalkii, T. Hutak, O. Rojas, S. M. de Souza, and O. Derzhko, Towards low-temperature peculiarities of thermodynamic quantities for decorated spin chains, arXiv:1908.06419.
 - [20] O. Rojas, J. Strečka, M. L. Lyra, and S. M. de Souza, *Phys. Rev. E* **99**, 042117 (2019).
 - [21] S. Buhbrandt and L. Fritz, *Phys. Rev. B* **90**, 094415 (2014).
 - [22] A. Otsuka, D. V. Konarev, R. N. Lyubovskaya, S. S. Khasanov, M. Maesato, Y. Yoshida, and G. Saito, *Crystals* **8**, 115 (2018).
 - [23] M. Mambrini, J. Trébosco, and F. Mila, *Phys. Rev. B* **59**, 13806 (1999).
 - [24] O. Rojas and F. C. Alcaraz, *Phys. Rev. B* **67**, 174401 (2003).
 - [25] M. Maksymenko, O. Derzhko, and J. Richter, *Acta Physica Polonica A* **119**, 860 (2011); M. Maksymenko, O. Derzhko, and J. Richter, *Eur. Phys. J. B* **84**, 397 (2011).
 - [26] V. Ohanyan, *Physics of Atomic Nuclei* **73**, 494 (2010).

[27] D. Antonosyan, S. Bellucci, and V. Ohanyan, Phys. Rev. B **79**, 014432 (2009).